Multiscale Surrogate-based Framework for Reliability Analysis of Unidirectional FRP Composites

Sadik L. Omairey[a]*, Peter D. Dunning[a], and Srinivas Sriramula[ab]
[a] School of Engineering, University of Aberdeen, AB24 3UE, United Kingdom
[b] Lloyd's Register Foundation (LRF) Centre for Safety & Reliability Engineering, University of Aberdeen, Aberdeen, AB24 3UE, United Kingdom
* Corresponding author: s.omairey@abdn.ac.uk, https://www.abdn.ac.uk/engineering/people/profiles/s.omairey

Abstract. In this paper, a Finite Element-based surrogate model is developed to efficiently estimate stiffness properties of unidirectional composite laminas, while accounting for geometric and material property uncertainties at micro, meso and laminate scale, all within a probabilistic framework. In the multi-scale build-up nature of composites, uncertainties occur in material properties and geometric characteristics. These uncertainties present a challenge in estimating composite material properties. The currently available property estimation/homogenisation tools are mainly divided into two categories: analytical methods constrained by configuration assumptions, and numerical homogenisation using Finite Element Analysis (FEA). The latter is more flexible and accurate, but computationally expensive. Hence, this paper develops a surrogate model based on a limited number of experimental FEA data points. Additionally, a transition phase is developed between micro and laminate scales that enables modelling of spatially varying uncertainties. As a result, this framework significantly decreases analysis duration compared with FEA techniques, and, because it is derived from FEA data points, can accurately represent a wide range of uncertainties.

Keywords: Composites; Uncertainty; RVE Homogenisation; Stiffness; Surrogates; Reliability.

1. Introduction

Composite materials are being widely used in many industries for the improved stiffness-to-weight ratio compared with alloys. However, the multi-phase structure and the manufacturing process of composites allows many material and geometrical uncertainties to occur [1-8]. As a result, composites are often designed deterministically using high factors of safety to avoid failure, which is considered conservative and restricts the use of the composites [9-11]. To avoid imposing such high factors of safety, it is important to account for system uncertainties by propagating their effect between the component's scales. Thus, a clear understanding of the overall composite properties under all uncertainties can be obtained. Clarifying this could lead to safer designs and more efficient use of composites, which can be achieved using a probabilistic design approach [10, 12-14]. Such an approach requires a reliable and accurate analysis method that can analyse the effect of various uncertainties on design performance. Monte Carlo simulation (MCS) is one method to find the solution of stochastic problems for its simple and direct implementation [8, 15]. It generates uncertainties in the form of random properties based on their statistical properties. To estimate composite properties and propagate the effect of these uncertainties, they are substituted in a homogenisation model, which is a common approach to designing parts with composite materials, as it provides an estimate for the effective elastic properties at different scales. Homogenisation methods are mainly divided into two categories: 1) Analytical methods, i.e. Rule of Mixtures [16] and Mori–Tanaka [17], and 2) Numerical homogenisation using Finite Element Analysis (FEA). The latter is more flexible and allows analysing a wide range of composite configurations, compared with the analytical methods that are constrained by assumptions and material property limitations [14, 18, 19].

The use of FEA-based homogenisation involves identifying a Representative Volume Element (RVE); one of its first definitions states that it should contain a sufficient number of inclusions and be typical of the mixture on average [20]. The balance between an RVE's computational efficiency and the range of uncertainties it can model is a key challenge in composites design. Some researchers used a small RVE, i.e. modelling only one or two fibres surrounded by a matrix phase. However, other studies, which investigated failure, or assessed the effect of defects, used larger RVEs with many fibres, to be able to capture more information [4, 21-25]. However, these studies did not require analysing a large number of RVEs, whereas many analyses are required to probabilistically estimate properties and reliability using MCS. Therefore, to reduce the computational cost, efficient surrogate models are used to transform FEA into analytical approximations, without a significant loss of accuracy [19, 26, 27].

For instance, Sobey et al. [28] used a surrogate modelling technique to estimate RVE properties under the effect of uncertain constituent material properties. Surrogates were constructed using FEA sample points while

each RVE contained a single fibre surrounded by matrix phase. In another uncertainty quantification and propagation study by Bostanabad et al. [29], the computationally expensive meso and micro scale homogenisation FEA, as part of a multiscale simulation method, were replaced by a metamodel generated and trained using data samples, enabling prediction of the stiffness matrix with less than 1% error compared with FEA results. The sources of uncertainty in this study were yarn angle, fibre volume ratio (V_f), and fibre misalignment angles. Another recent study by Wu et al. [30] analysed a wide range of SEM images to create a micro-structure generator that provided virtual micro-samples for numerical analyses. Thus, the study focused on fibre randomness, while considering deterministic constituent material properties. Wu et al. used a multi-level computational homogenisation method to extract the meso-scale response of larger RVEs in an efficient way using 2D interpolation of material properties within a two-step computational homogenisation framework. The study also examined the effect of different boundary conditions, and it concluded that periodic boundary conditions are an accurate choice for their multi-level computational homogenisation approach. Additionally, previous work by the authors [14] used FEA RVE homogenisation to develop an efficient polynomial-based surrogate model that is capable of accounting for micro-scale geometric and material uncertainties at the micro-scale (see Fig. 1(b)), while minimising the use of expensive FEA RVE homogenisation, making it feasible to use within a MCS-based probabilistic study. This was achieved using two-fibre RVEs containing a randomly stacked fibre at the centre, and periodicity was maintained at the RVE surfaces. Data points were generated for a limited number of RVEs allowing the construction of regression fit surrogate models. These were used to estimate stiffness properties and reliability using MCS.

The novel contributions of this study are: 1) creating a computationally efficient framework that is capable of capturing more uncertainties between the micro and laminate scale, compared with the available frameworks and techniques. 2) producing a new inclusive material representation by developing a transition meso-scale as seen in Fig. 1(c). 3) associating random RVEs by means of several spatial correlation criteria to form a larger RVE that captures a wider frame of the material uncertainties. This is achieved by developing another level of efficient surrogate model using low fidelity FEA, making it suitable for reliability calculations using MCS.

The structure of this paper starts with the methodology in Section 2. Then, Sections 3 and 4 validate and discuss the results using the developed method, compared with FEA results and the previous framework. Section 5 highlights the key findings and draws conclusions from the validation and application examples.

2. Methodology

Our previous framework computed the homogenised stiffness properties of randomly generated RVEs using FEA data points obtained using an in-house periodic RVE homogenisation tool - EasyPBC [31]. Each RVE only contained two fibres. The framework uses the FEA data points to create polynomial-based surrogate models that relate uncertainties to their effect on stiffness properties. For a given sample of the uncertain parameters, the surrogate model is used to efficiently compute the homogenised stiffness properties, which are then applied to a single lamina ply, as can be seen in Fig. 1(b). However, this framework is limited because it assumes no spatial variation in uncertain parameters within a single lamina ply.

In order to simulate realistic spatial variation of uncertainties, a second scale of RVEs is introduced, which is a Larger RVE (LRVE) constructed using several micro-scale RVEs. Therefore, the proposed LRVE can be used as a meso-scale RVE that allows spatial variation in uncertainties, resulting in a more realistic representation of the higher scale, compared with the use of conventional micro-scale RVEs (See Fig. 1(c)).

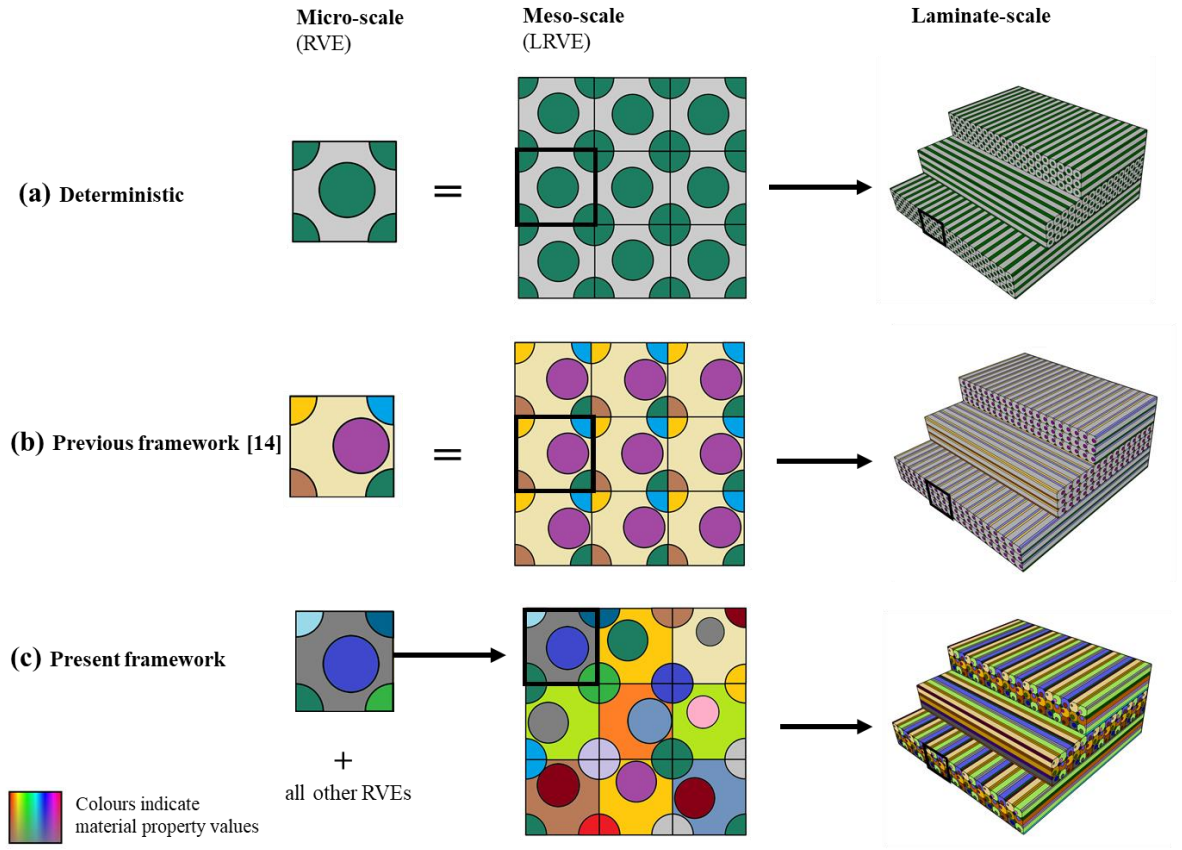

Fig. 1. The current and previous micro-meso upscaling approaches.

The overall algorithm of the developed framework starts with identifying uncertainties and their statistical properties, generating micro-scale RVEs, then the LRVE, assigning stiffness properties to laminate plies and finally including laminate-scale uncertainties, such as ply thickness and orientation. Each element is explained in the following sections.

2.1. Uncertainties

In this study, *E*-glass fibre-epoxy composite is selected to investigate the developed framework. Uncertainties for this example are presented within two categories: the first is the micro and meso scale, this includes material properties along with fibre stacking, represented by radial displacement (r and θ, where the distance r is measured as a fraction of the RVE edge length, as shown in Fig. 3), and fibre volume ratio (V_f) in the form of uncertain fibre cross-sectional areas. The second category is within the laminate scale, it includes thickness, ply orientation and loading uncertainties. The assumed statistical properties of all the uncertainties are provided in Table 1, and are similar to values used and assumed in the literature [32-35].

Table 1. Material properties and uncertainties.

Property/ uncertainty	Fibre (*E*-glass)		Matrix (Epoxy)		Fibre-volume ratio V_f	Fibre stacking (r and θ)	Lamina ply thickness t	Lamina ply orientation θ_p	**Pressure load L (MPa)
	E_m (GPa)	v_m (ratio)	E_f (GPa)	v_f (ratio)					
Mean/ lower limit	72.45	0.25	4.0	0.3	0.52	RVE centre, 0°	0.5 mm, **0.53 mm and 0.44 mm	[0°/90 °]s, **[75°/45°]s	0.05
Distribution	Normal	Normal	Normal	Normal	Normal	Uniform	Normal	Normal	Normal
CoV/ limits	5%	5%	5%	5%	5%	r: 0-0.08* θ: 0°-360°	5%	5 °	5%
Categories	Micro and Meso scales						Laminate scale		

**Fraction of the RVE edge length. ** For the numerical example.*

2.2. Micro-scale RVE

RVEs with nominal hexagonal fibre packing are used in this study, each containing two fibres in total (full fibre and four quarters, as shown in Fig. 1(a)). Additionally, it is assumed that the fibres and the matrix are fully-bonded and there are no voids. Each RVE is subjected to micro-scale uncertainties, as summarised in Table 1, with some specific correlations and assumptions, which are explained below in Section 2.3. To estimate the effective properties of the composite within a probabilistic analysis, it is necessary to homogenise a significant number of randomly generated RVEs.

In this study, an open-source ABAQUS plugin, developed by the authors [31], is used for FEA RVE homogenisation. This method is widely used to predict the effective elastic properties of composite materials for its clear mechanical conception and simplicity [18, 19]. Additionally, the estimated properties using this tool are verified against other available established experimental data and commercial homogenisation software [31]. The plugin estimates these properties by applying node-to-node periodic conditions, at which deformed boundary surfaces can distort and no longer remain plane under applied displacements. These periodicity conditions are achieved by linking nodal degrees of freedom (DoF) as illustrated in Appendix A.

The RVE homogenisation is computationally expensive. Thus, the surrogate model is created to minimise their use. This model is mainly constructed by polynomial regression fits to identify the relationship between uncertainties and their effect on stiffness properties, using data points obtained by FEA. This approach was developed earlier [14], and is explained and assessed in Sections 2.4.1 and 2.4.2, respectively.

2.3. Meso-scale LRVE

Many studies that have investigated the effect of uncertainties on reliability use MCS to generate independent random uncertain RVEs for each sample. This approach is valid if spatial correlation is not considered and the estimated properties at the end of each MCS output represent the properties of a single point/region in the higher scale model. However, this is not the case in the proposed LRVE approach, as each MCS sample aims to accurately capture a larger portion of the material at the meso-scale by gathering several neighbouring micro-scale RVEs, as seen Fig. 1(c). Therefore, the following criteria and assumptions are implemented to achieve a spatial correlation between the random RVEs used to generate a specific LRVE.

2.3.1. Fibre properties and arrangement

As stated earlier, the micro-scale RVE contains two fibres in total. The randomness in material properties of neighbouring fibres within each RVE is uncorrelated, as they are independent. However, when it comes to modelling an RVE within a LRVE, corner fibre quarters meet up with neighbouring RVE corners. As a result, assuming a random property value for each adjacent fibre quarter is not an accurate representation. Thus, the proposed LRVE framework accounts for this by assigning the same fibre material property values to all adjacent corner fibre sections, creating a type of relationship between individual RVEs and their surroundings. This can be seen in the colour mapping in Fig. 2 and Fig. 1(c).

On the other hand, the framework divides fibres into two categories: fixed fibres represented by the RVEs' four fibre corner quarters; geometrically speaking, these quarters remain in place and have the same diameter to preserve continuity with its neighbours. The second category is the central non-fixed fibres, which can shift and experience geometric change within the RVE to allow modelling of stacking (r and θ) and V_f ratio uncertainties, without violating continuity, as can be seen in Fig. 2.

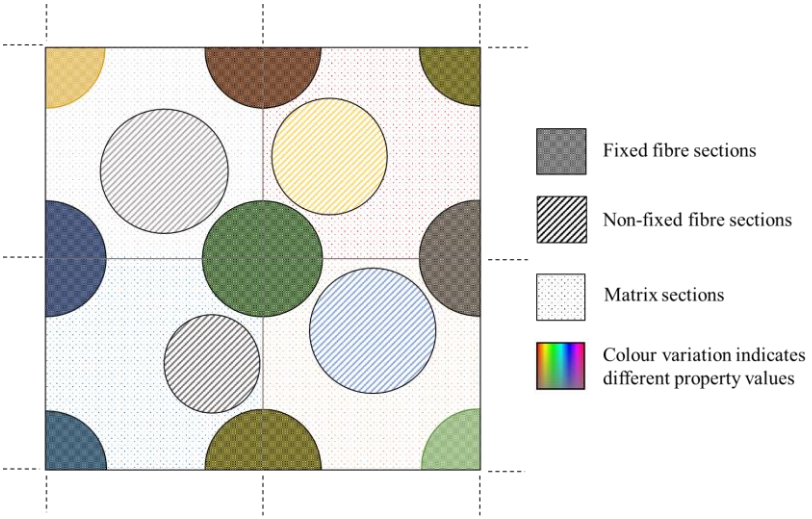

Fig. 2. Assuming fixed and non-fixed fibres to maintain periodic RVEs' boundaries while including geometric and constituent material properties uncertainties.

The generation of the non-fixed fibre location and size (or V_f ratio) is controlled to ensure that no RVE will have overlapping fibre sections (which is unrealistic). This is achieved by checking and adjusting the values of both the random stacking radius and the non-fixed fibre radius as explained in Fig. 3.

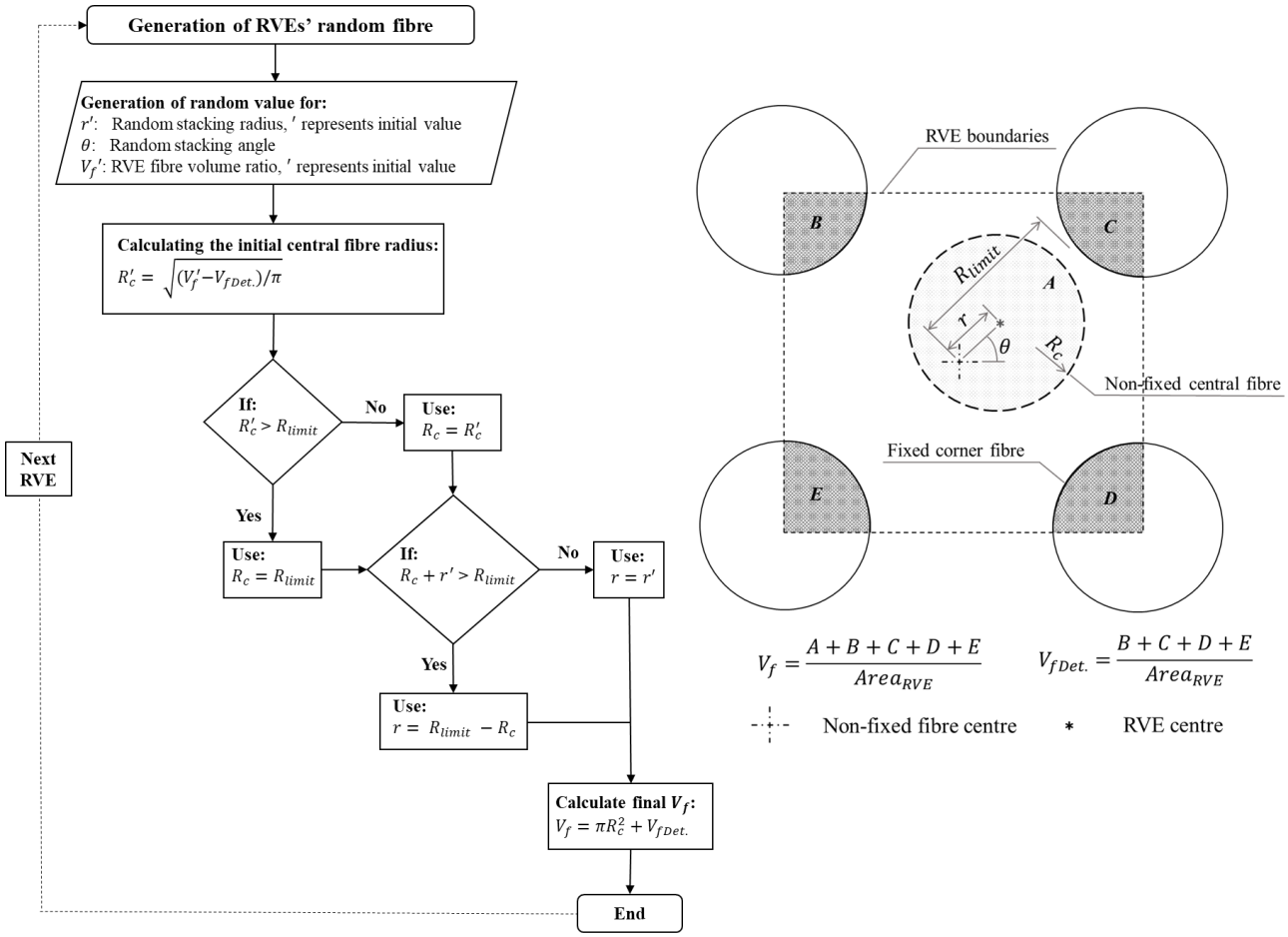

Fig. 3. The algorithm used to generate RVEs' central fibre uncertainties: V_f, r and θ.

2.3.2. Matrix property normalisation

The matrix material surrounding fibre filaments is a continuous media, so it is unrealistic to have sharp jumps in its property values, as any change in its properties should be smooth and gradual. Therefore, assuming random values for neighbouring RVEs is not a realistic representation. In the proposed framework, matrix material property randomness is smoothed out using an image processing concept as can be seen in Fig. 4. A smoothing blur kernel (see Eq. 1) is multiplied by matrix uncertainties within a shifting 3×3 RVE frame to estimate each RVEs' normalised matrix stiffness properties. In order to cover the entire desired LRVE area, there is a need to generate random variables for LRVE edges. It is important to note that this averaging technique will not significantly affect the overall statistical distribution of the matrix material property, as can be seen in the mean values shown in Fig. 4.

The normalisation region size (3×3 RVEs) for the proposed method is not backed by experimental data. However, if such data are available, then the developed framework can alternatively use a larger frame size, weighted kernels, or other correlation methods.

$$Blur\ Kernel = \frac{1}{9}\begin{bmatrix} 1 & 1 & 1 \\ 1 & 1 & 1 \\ 1 & 1 & 1 \end{bmatrix} \tag{1}$$

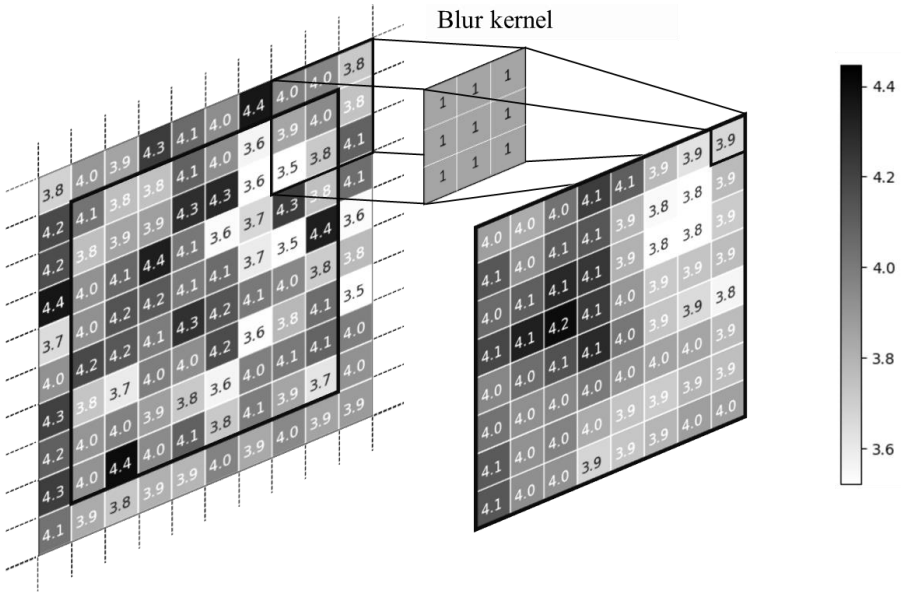

10x10 RVEs, Sample μ = 3.893 GPa 8x8 RVEs, Sample μ = 3.891 GPa

Fig. 4. Smoothing the random matrix property values using the blur kernel.

2.4. Surrogate models

In this study, a series of surrogate models are used to develop an efficient FEA-based stiffness reliability framework. These models are divided into two types: 1) Polynomial regression fits to estimate the effect of uncertainties on properties. 2) Accumulation of independent effects to estimate the overall effective elastic properties of the RVE and LRVE. These surrogate models approximate the influence of uncertain input material property values on output homogenised properties and are explained as follows:

2.4.1. Micro-scale RVE surrogate models

Polynomial regression fits are created to form the relationship between uncertainties and their effect on elastic properties, using data points obtained by the FEA RVE homogenisation (data points are explained in Section 3.2). Due to the fact that most uncertainties are largely dependent on V_f, their surrogate models are 3D surface fits of the uncertainty, V_f, and the effect on stiffness. Whereas corner fibre uncertainties are found to be almost independent of V_f and their effects on stiffness are interpolated using 2D fits, as can be seen in Fig. 5.

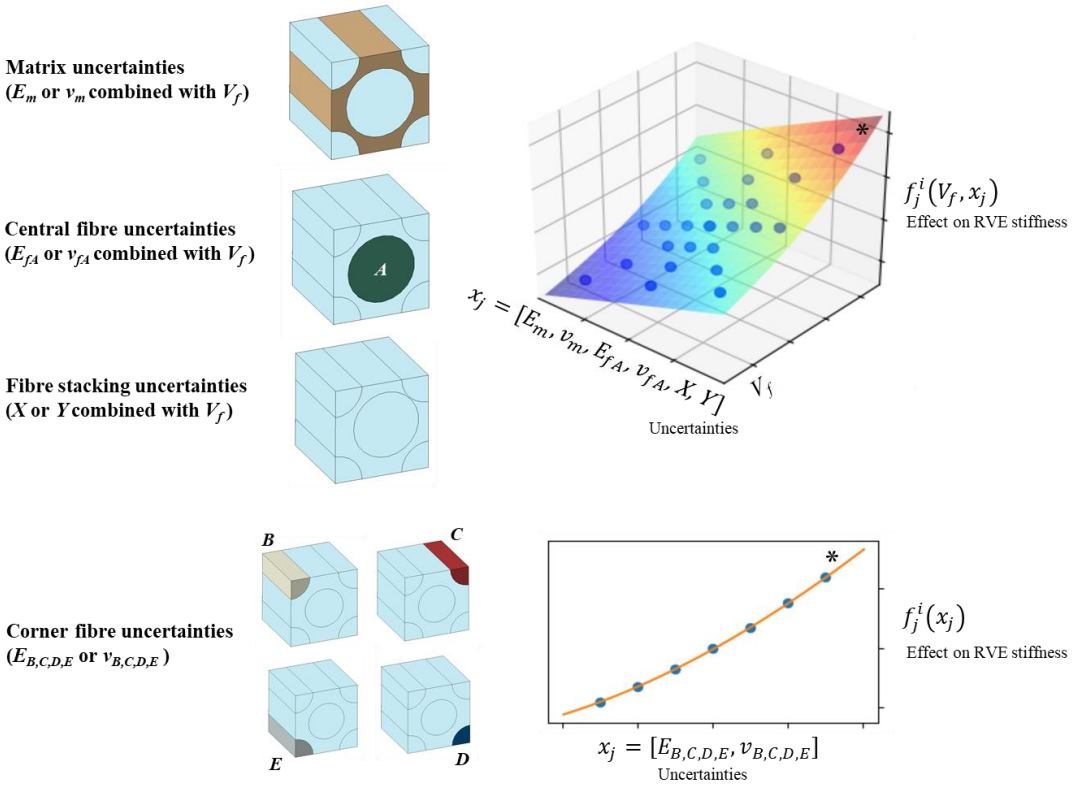

Fig. 5. Micro-scale surrogate models for material and geometrical uncertainties.

These Polynomial regression fit surrogate models output the estimated effect of individual uncertainties. The effects are accumulated using Eq. 2 to estimate the homogenised properties of each random RVE.

$$E^i{}_{\overline{RVE}_l} = E^i{}_{Det} + \sum_{j=1}^{N} f_j^i(x_j) \tag{2}$$

Where $E^i{}_{\overline{RVE}_l}$ is one of the approximated elastic properties, i, for RVE l, $E^i{}_{Det}$ is the deterministic value of the elastic property i, N is the number of uncertain parameters (x_j) and $f_j^i(x_j)$ is a polynomial that links the value of uncertain parameter j with a change in the elastic property i (relative to deterministic value). An example on the generation of the polynomial regression fit using the data points is shown in Fig. 6 (for matrix E_m, and V_f uncertainties). In this figure, the selected set of data points is referred to as *DPS 3* (explained Section 3.2), which uses FEA homogenisation data at the mean (μ), and eight more points offset around the mean by three standard deviations (3σ).

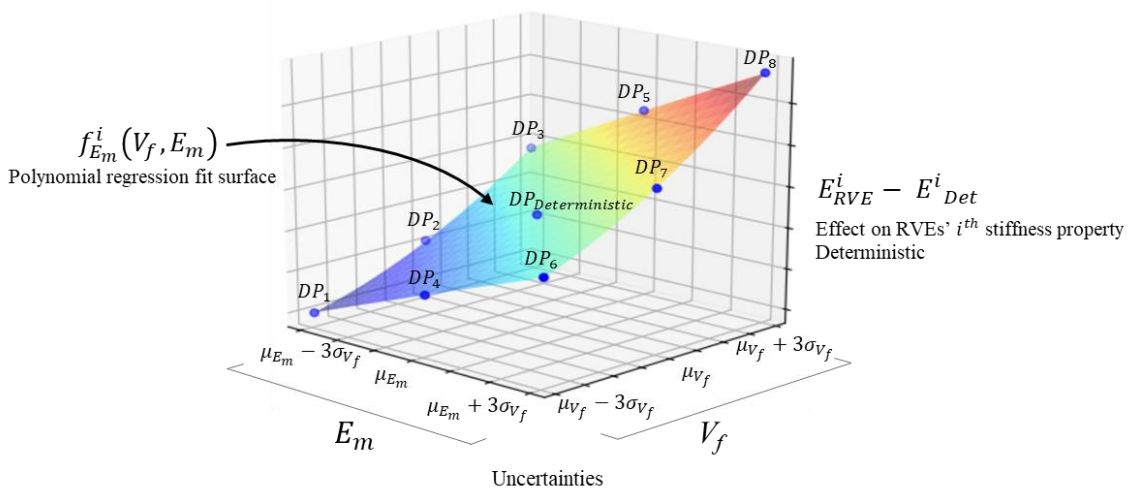

Fig. 6. The use of data points to interpolate the polynomial regression fit surface. In this case for the effect of matrix stiffness uncertainty (E_m,) and V_f,.

2.4.2. Meso-scale LRVE surrogate models

The estimated properties of the micro-scale RVEs go through two proposed techniques to estimate the properties of the LRVE. The first technique is a combination of polynomial regression fits and effect accumulation. In the polynomial regression fit stage, the surrogate model is constructed using low fidelity LRVE FEA data points. These LRVE data points contain a property-altering RVE surrounded by RVEs with deterministic properties. Once constructed, the homogenised properties of all individual random RVEs (computed using the surrogate model from Section 2.4.1) are substituted in a generated 2D surrogate model to estimate the corresponding dependent effect on the LRVE. In the second stage, the corresponding effects are accumulated to estimate the elastic properties of the LRVE as explained in Eq. 3 and Fig. 7.

$$E^i{}_{LRVE} = E^i{}_{Det\ LRVE} + \sum_{l=1}^{L} f_s^i\left(E^i{}_{\overline{RVE}_l}\right) \tag{3}$$

Where $E^i{}_{LRVE}$ is one of the approximated elastic properties of the LRVE, $f_s^i\left(E^i{}_{\overline{RVE}_l}\right)$ is a polynomial that links the value of a single $\overline{RVE}_l$ property with the effect on the LRVE, L is the total number RVEs within an LRVE, and $E^i{}_{Det\ LRVE}$ is the deterministic value of elastic property i ($E^i{}_{Det\ LRVE} = E^i{}_{Det}$). Although RVEs generated and arranged within the LRVE are spatially correlated, as explained in Section 2.3, this approach accumulates RVE's effects regardless of their location within the LRVE.

Therefore, a second technique is proposed that accounts for RVE location by using a multi-stage homogenisation process. The idea is to homogenise 2×2 configurations of neighbouring RVEs, which then form the homogenised properties for the following stage. This process continues in multiple stages until reaching the desired LRVE size. To account for RVE location, the polynomial-based surrogate model includes extra terms for: horizontal (f_h), vertical (f_v), and diagonal effects (f_d). These surrogate models are again generated using low fidelity FEA data points, and their effects are summed similar to the first technique, as shown in Eq. 4, 5 and Fig. 7. The efficiency of both techniques is assessed in Section 3.3 to select and use the most suitable technique within the overall probabilistic framework.

$$E^i{}_{Stg.1_C} = E^i{}_{Det\ LRVE} + \sum f_s^i\left(E^i{}_{\overline{RVE}_{A,B,C,D}}\right) + \sum f_h^i\left(E^i{}_{\overline{RVE}_{A-B,C-D}}\right) + \sum f_v^i\left(E^i{}_{\overline{RVE}_{A-D,B-C}}\right) + \sum f_d^i\left(E^i{}_{\overline{RVE}_{A-C,B-D}}\right) \tag{4}$$

$$E^i{}_{Stg.2} = E^i{}_{LRVE} = E^i{}_{Det\ LRVE} + \sum f_s^i\left(E^i{}_{Stg.1_{A,B,C,D}}\right) + \sum f_h^i\left(E^i{}_{Stg.1_{A-B,C-D}}\right) + \sum f_v^i\left(E^i{}_{Stg.1_{A-D,B-C}}\right) + \sum f_d^i\left(E^i{}_{Stg.1_{A-C,B-D}}\right) \tag{5}$$

Where $E^{i}{}_{Stg.1_C}$ is one of the approximated elastic properties of the 1st stage of the LRVE multi-stage homogenisation, whereas $E^{i}{}_{Stg.2}$ represents the approximated properties of the second stage. $f^{i}_{s,h,v,d}\left(E^{i}{}_{\overline{RVE}_{A,B,C,D}}\right)$ are the polynomials that link the property's value of single (f_s) and the spatial effect of horizontal (f_h), vertical (f_v), and diagonal (f_d) of four RVEs (*A,B,C,D* following the order in Eq. 4 and 5), to estimate the properties of the 2nd stage regions (Fig. 7). If an 8×8 LRVE is used then a third stage is required; similarly, a fourth stage for a 16×16 LRVE, and so on.

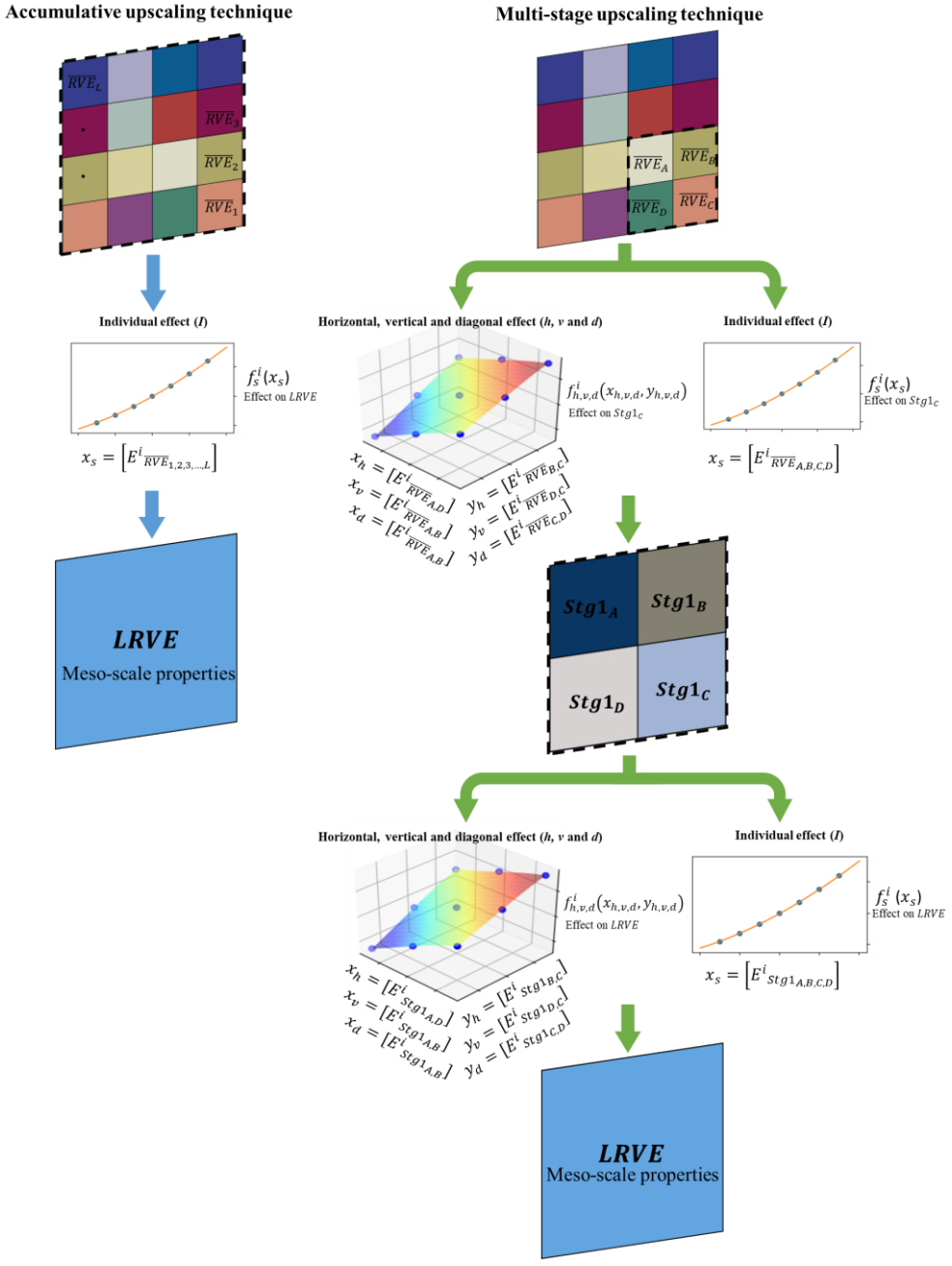

Fig. 7. Accumulative and multi-stage meso-scale surrogate modelling techniques.

3. Framework validation

The developed framework aims to evaluate composites stiffness reliability in an efficient and accurate manner by constructing LRVEs and using FEA-based surrogate models. Before carrying out the reliability study, several aspects of the developed technique are examined.

3.1. FEA discretisation study

To estimate the amount of error associated with using the developed surrogate models, it is important to account for the numerical error associated with the finite element discretization. To estimate this for the micro-scale, deterministic RVEs were modelled using four different mesh sizes to compute the effective stiffness properties. A trend line is used to estimate the true elastic properties by extrapolating to a mesh size of zero. The estimated true values are then used as a reference point to calculate an estimated error for each mesh size, as shown in Fig. 8 for Young's modulus in the 1-direction (E_{11}), and listed in Table 3 for the other stiffness properties. Based on this study, a maximum mesh size of 0.02 (fraction of the RVE's edge length using linear wedge elements) is used for RVE discretisation, as it provides an acceptable balance between accuracy and computational time.

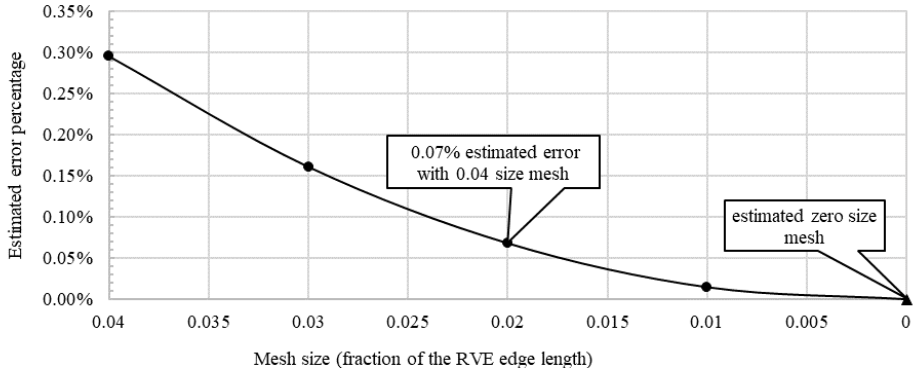

Fig. 8. Four-point mesh convergence line with the estimated error plotted against mesh size for E_{11}.

In addition to the above micro-scale FEA error estimation, the use of low fidelity FEA to create the surrogate model for the LRVEs' meso-scale (Section 2.4.2) is examined by generating a random LRVE, as shown in Fig. 9, and estimating its stiffness properties using: 1) a high fidelity FE model that explicitly meshes all details with the same mesh size as the individual RVEs, and 2) a low fidelity model that does not explicitly model all detail, but instead simply assigns regions of elements with properties derived from the micro-scale surrogate models (Section 2.4.1). The average absolute error between the effective properties is observed to be 0.2%. Similar error magnitudes are observed in other randomly generated high and low fidelity LRVEs. Thus, it was concluded that using the low fidelity model was accurate enough to generate data points for the LRVE surrogate models.

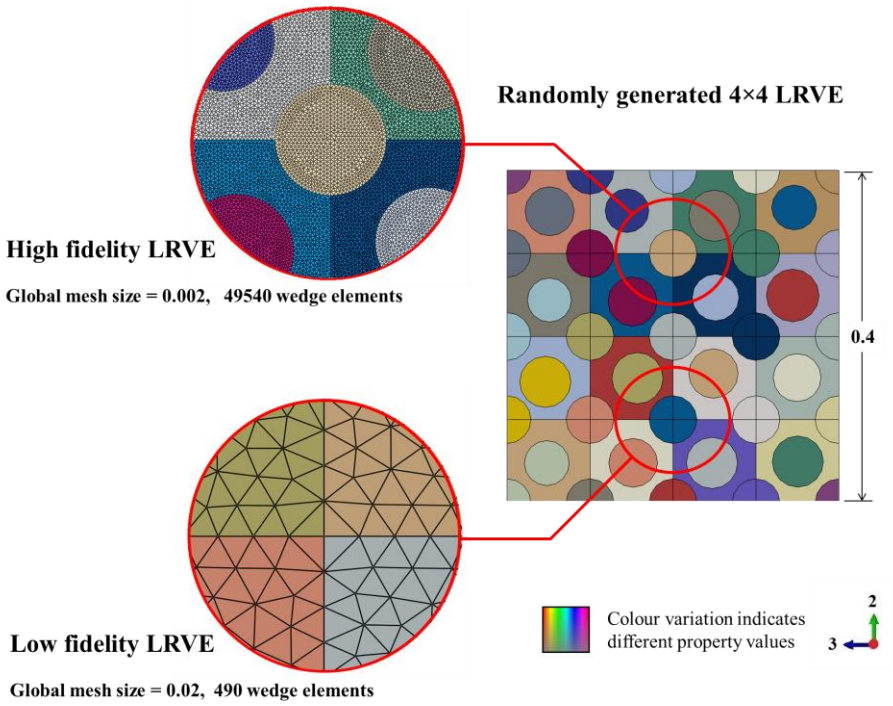

Fig. 9. A randomly generated 4×4 LRVE modelled and analysed with a low and high fidelity FEA.

3.2. Data points

To examine the effect of the number and distribution of FEA data points on the accuracy of the surrogate models, three different sets of points are used (*DPS*1, *DPS*2, *DPS*3), which are defined by the number of standard deviations (σ) from the mean for constituent material property uncertainties, or percentage of mean for geometric uncertainties and homogenised properties used in the LRVE, as seen in Table 2.

Table 2. Space of FEA data points.

Data points set	3rd Data points set (*DPS*3)						
		2nd Data points set (*DPS*2)					
			1st Data points set (*DPS*1)				
Material property uncertainties	$Mean - \sigma$	$Mean - 2\sigma$	$Mean - 3\sigma$	$Mean$	$Mean + 3\sigma$	$Mean + 2\sigma$	$Mean + \sigma$
Geometrical uncertainties	$Mean * 0.9$	$Mean * 0.8$	$Mean * 0.7$	$Mean$	$Mean * 1.3$	$Mean * 1.2$	$Mean * 1.1$
LRVE properties	$Mean * 0.9$	$Mean * 0.8$	$Mean * 0.7$	$Mean$	$Mean * 1.3$	$Mean * 1.2$	$Mean * 1.1$

All three sets of data points are analysed using the RVE homogenisation method; then the micro-scale surrogate models are generated. The error accompanying the use of the generated surrogate model sets in estimating the properties of 64 random RVEs (simulating a set of RVEs required for an 8×8 LRVE) is predictable by comparison with the FEA homogenisation of each of the 64 RVEs. Table 3 illustrates this in the form of error mean (μ) and standard deviation (σ) for each stiffness property, and the total number of data points and approximate duration required to generate the data using a 1 CPU.

Table 3. Error percentages associated with the use of different data points set sizes.

Data points set	DPS3						Estimated FEA numerical discretization error % (for a mesh size of 0.02 as shown in Fig. 8)
	DPS2						
	DPS1						
Number of data points used	53		97		141		
Approx. data points off-line processing time	~ 5 hours		~ 9 hours		~ 13 hours		
Error % mean (μ) and standard deviation (σ) compared with 64 random FEA RVEs	μ	σ	μ	σ	μ	σ	
E_{11}	0.00	0.00	0.00	0.00	0.00	0.00	0.07
E_{22}	0.62	0.27	0.05	0.05	0.03	0.04	0.01
E_{33}	0.61	0.30	0.05	0.04	0.03	0.04	0.02
G_{12}	0.59	0.26	0.06	0.05	0.04	0.04	0.01
G_{13}	0.57	0.32	0.05	0.05	0.04	0.04	0.02
G_{23}	0.13	0.10	0.04	0.04	0.04	0.03	0.07
v_{12}	0.06	0.05	0.06	0.05	0.06	0.05	0.01
v_{13}	0.05	0.05	0.05	0.05	0.05	0.05	0.01
v_{23}	0.24	0.13	0.03	0.02	0.02	0.02	0.13

It is clear that error values are very small using surrogate models constructed by *DPS*3 (which includes both *DPS1* and *DPS*2). For this reason, *DPS*3 is selected to create the homogenising micro-scale RVEs surrogate model (section 2.4.1) to output the properties of the meso-scale LRVE. It is important to note that this set will be constructed once as an offline process for each type of material and selected uncertain values.

3.3. Meso-scale surrogate models and LRVE size

In order to assess the effectiveness of the two proposed meso-scale LRVE surrogate modelling techniques and select the most suitable, random sets of LRVEs are generated with uncertain properties derived using *DPS*3. The results of using each meso-scale surrogate modelling technique (accumulative and multi-stage) are compared with low fidelity FEA of the same randomly generated LRVEs. In this process, three sizes of LRVEs are investigated: 2×2, 4×4 and 8×8 RVEs, and for each size 100 random LRVEs are generated. The comparison is presented in the form of mean error for each stiffness property, as shown in Fig. 10.

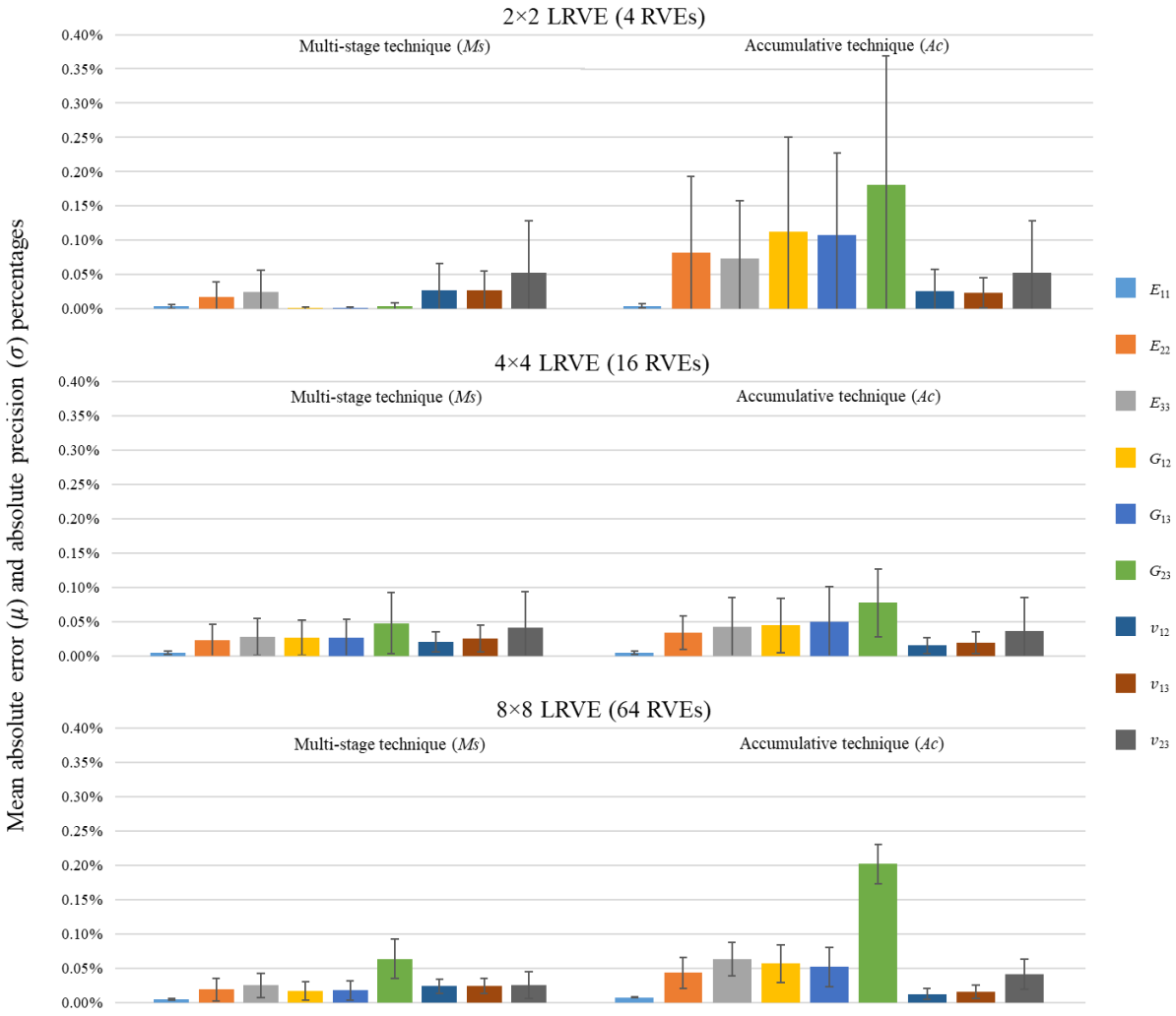

Fig. 10. The statistical performance of multi-stage and accumulative technique for three LRVE sizes.

To quantitatively compare the performance of multi-stage and accumulative techniques, the probability that the error of the multi-stage technique ($\delta_{Ms} \sim N(\mu_{Ms}, \sigma_{Ms}^2)$) is less than the accumulative technique error ($\delta_{Ac} \sim N(\mu_{Ac}, \sigma_{Ac}^2)$) is estimated using the relations shown in Eq. 6 below:

$$\left.\begin{aligned} &P(\delta_{Ms} < \delta_{Ac}) \;=\; P(\delta_{Ms} - \delta_{Ac} < 0) \\ &\text{If } Q = \delta_{Ms} - \delta_{Ac}, \text{ then } Q \sim N(\mu_{Ms} - \mu_{Ac},\; \sigma_{Ms}^2 + \sigma_{Ac}^2) \text{ and:} \\ &P(Q < 0) = \Phi\left(\frac{0 - \mu_Q}{\sigma_Q}\right) \end{aligned}\right\} \qquad (6)$$

It is important to note that the relations in Eq. 6 are valid for normal distributions (N and Φ). Therefore, the distributions of errors are checked for their normality using a Q-Q test [36]. It is observed that a majority of them follow a normal distribution, except several sets for 2×2 LRVE, due to having a fewer number of RVE elements compared with 4×4 and 8×8 LRVEs. Nevertheless, the errors in these sets are seen to follow a normal distribution at slightly lower levels of significance, which is considered acceptable for the purposes of this study. Based on the probabilities $P(Q < 0)$ for examined LRVE size shown in Fig. 11, it is concluded that the multi-stage technique performs better across most properties except Poisson's ratios v_{12} and v_{13}, as they appear to be insensitive to the diagonal effect. Thus, within the overall framework, only these properties will be estimated using the accumulative technique, the rest of the properties will be evaluated using the multi-stage technique.

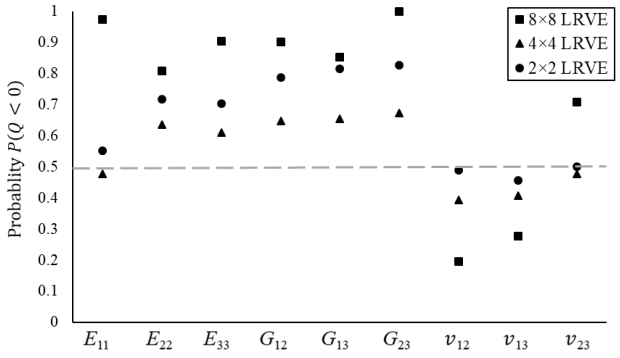

Fig. 11. The probabilities of the multi-stage technique mean error values being smaller than of the accumulative.

It is important to note that the selection of LRVE size for composite representation requires considerations of lamina thickness in parallel with the selected boundary conditions. In this particular study, it is assumed that even the 8×8 LRVE is considerably smaller than the lamina thickness. Thus, it is suitable to apply periodic boundary conditions.

4. Framework overview and application

4.1. Framework overview

The proposed framework that efficiently estimates stiffness properties of unidirectional composite laminas, while accounting for spatial geometric and material property uncertainties at micro, meso and laminate scale is demonstrated by assessing the stiffness reliability of composite laminates. Based on the results of the validation section, the final algorithm and implementation of the developed framework is illustrated in Fig. 12.

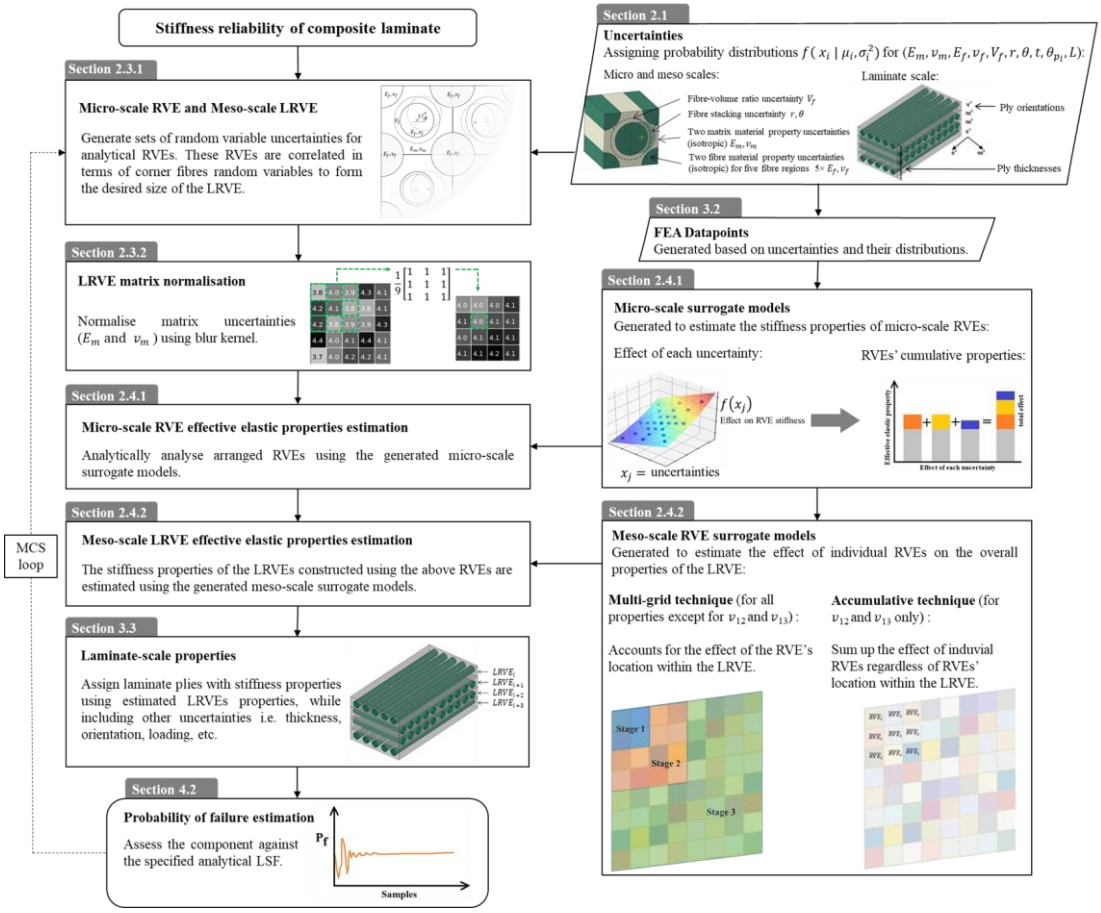

Fig. 12. Proposed framework flowchart for evaluating laminate probabilistic stiffness performance.

4.2. Application examples

Analytical and numerical-based examples are used to assess the developed framework. The first example is a set of four specially orthotropic 0.5 mm thick laminas, symmetrically arranged about the laminate mid-surface (see Fig. 13), presented to assess buckling stiffness reliability. The properties of each plie are derived from a random meso-scale LRVE. Thus, for each MCS sample, there are four lamina stiffness properties derived from four different LRVEs, which are then used with classical laminate theory. On the other hand, in addition to micro and meso-scale randomness, lamina ply thickness (t) and ply orientation (θ_p) are introduced as uncertainties and their statistical properties are provided in Table 1. These uncertainties are introduced at the ply level rather than laminate, with no-correlation with V_f ratio. It should be noted that the introduction of ply orientation uncertainty will contradict the specially orthotropic orientation concept. However, it is observed that buckling response for all randomly generated laminates can be accurately estimated using the same expression for orthotropic laminates, as they satisfy the relations shown in Eq. 7 [10].

$$\frac{D_{16}}{\sqrt[4]{D_{11}^3 D_{22}}} < 0.2, \quad \text{and} \quad \frac{D_{26}}{\sqrt[4]{D_{22}^3 D_{11}}} < 0.2 \tag{7}$$

Where D_{ij} represent laminate bending stiffnesses components, as presented in Appendix B.

For this particular laminate configuration, the required stiffness components are only D_{11}, D_{12}, D_{22} and D_{66}; hence, simplifying limit state function (LSF) calculations. MCS is used to randomly generate uncertainties, X, for all scales, and substitute them in the developed surrogate models to compute stiffness properties (Sections 2.4.1 and 2.4.2). These are then used with classical laminate theory [37, 38] to calculate the D_{ij} stiffness terms along with the effect of laminate-scale uncertainties. The LSF is evaluated for each randomly generated laminate, as detailed in Eq. 8 [39], to estimate the probability of failure by assuming that failure occurs once serviceability limits are reached: $P_f = P[g(X) \leq 0]$.

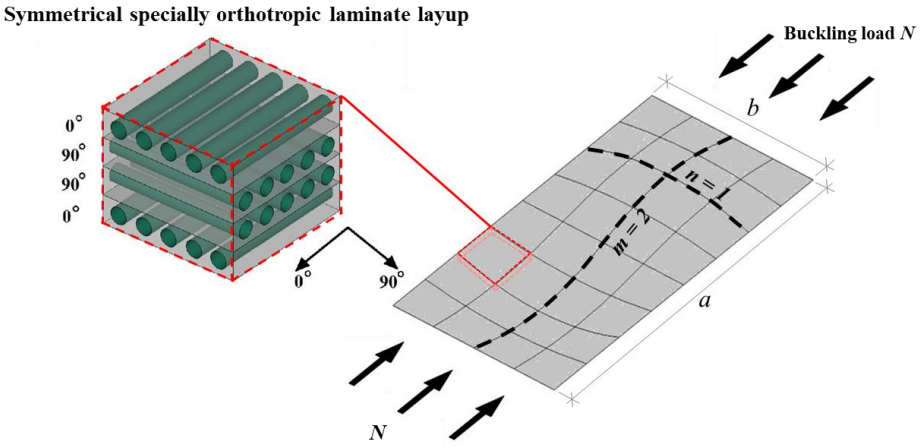

Fig. 13. Symmetrically specially orthotropic laminate subjected to buckling loading conditions.

$$g_b(X) = N - N_{LS} = \pi^2 \left[D_{11} \left[\frac{m}{a}\right]^2 + 2(D_{12} + 2D_{66}) \left[\frac{n}{b}\right]^2 + D_{22} \left[\frac{n}{b}\right]^4 \left[\frac{a}{m}\right]^2 \right] - N_{LS} \tag{8}$$

The above applies for a simply supported symmetrical specially orthotropic laminate, where:

N_{LS}: Applied load per laminate width (155 N/mm when all uncertainties are considered, and 189 N/mm when lamina level uncertainties are ignored).

D_{ij}: Laminate stiffness components, calculated using random variables, X through surrogate models and *[ABD]* matrix stiffness calculations as presented in Appendix B.

m, n: The number of half wavelengths at 0° and 90°-direction respectively, m=2 and n=1 for buckling.

a, b: Laminate length (100 mm), and width (50 mm) respectively.

For the numerical example, the framework is used to assess the stiffness reliability of an optimised skewed propeller blade made of two symmetrical (four in total) laminas $[75^o/45^o]_S$, with the properties and uncertainties shown in Table 1. Additionally, this example includes a pressure load uncertainty. The stiffness LSF is defined is the maximum allowable deformation in the Z-direction (U_{LS}), which the blades' trailing edge will experience by the pressure load, thus, $P_f = P[(U_{edge} - U_{LS}) \leq 0]$. The position of the selected trailing edge node U_{edge} can be seen Fig. 14; U_{LS} value is $5.2\,mm$ when all uncertainties are considered, and $4.75\,mm$ when lamina level uncertainties are ignored. For the purpose of this example, a multivariate nearest-neighbour Python interpolation module [40] with 2,000 FEA data points are used to estimate the probabilistic stiffness response of the blade to extract U_{edge} values. The total number of uncertain variables is 33: 4×6 laminate stiffness properties, 4 ply thicknesses, 4 ply orientations and 1 loading input.

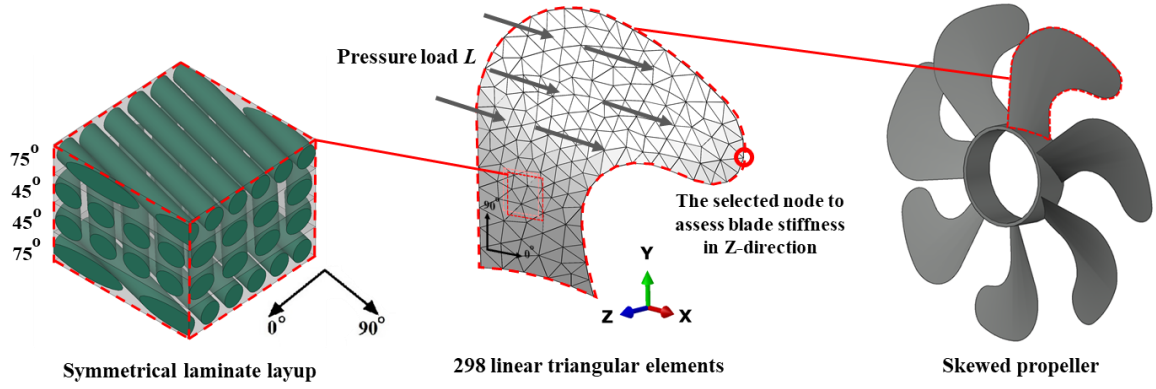

Fig. 14. Blade formed made of symmetric laminate subjected to pressure load.

Employing the developed framework, four meso-scale configurations are used to compute the stiffness reliability of the selected composite laminate examples, which are: 1×1 single RVE (Fig. 1(a)), 2×2, 4×4, and 8×8 LRVEs. The total number of MCS samples required (S) is estimated using the relation shown in Eq. 9 [41], targeting an initial probability of failure $P_f' = 10^{-3}$, 10% maximum allowable error (δ_{P_f}), and 80% confidence level (α).

$$S = \frac{P_f'(1 - P_f')}{\delta_{P_f}^2} Z_{(1+\alpha)/2}^2 = \frac{10^{-3}(1 - 10^{-3})}{(1 * 10^{-4})^2}(1.28)^2 \approx 160{,}000 \tag{9}$$

As the probability of failure is a binomial distribution and $nP_f > 5$, it is adequate to use Z to calculate the inverse of the standard normal cumulative distribution for the value $(1 + \alpha)/2$.

Stiffness reliability results are presented in Fig. 15, showing that for both examples, the probability of failure reduces as the size of the LRVE increases and that all sizes of LRVEs compute a lower P_f value, compared with using a single RVE (i.e. no meso-scale transition). This result can be explained because increasing the size of the representative unit leads to less variability of homogenised properties at the lamina-scale, thus reducing the chances of assigning extremely low stiffness values to the whole lamina that causes failure. This can be seen in Fig. 16 that plots the distribution of homogenised properties for the examined sizes along with their fitted normal distribution curve. Furthermore, if laminate uncertainties are not considered (similar if reduced), then the variation in P_f between different sizes of LRVEs and the single RVE is more noticeable, as can be seen in Fig. 17, which again is the case for both the analytical and numerical examples.

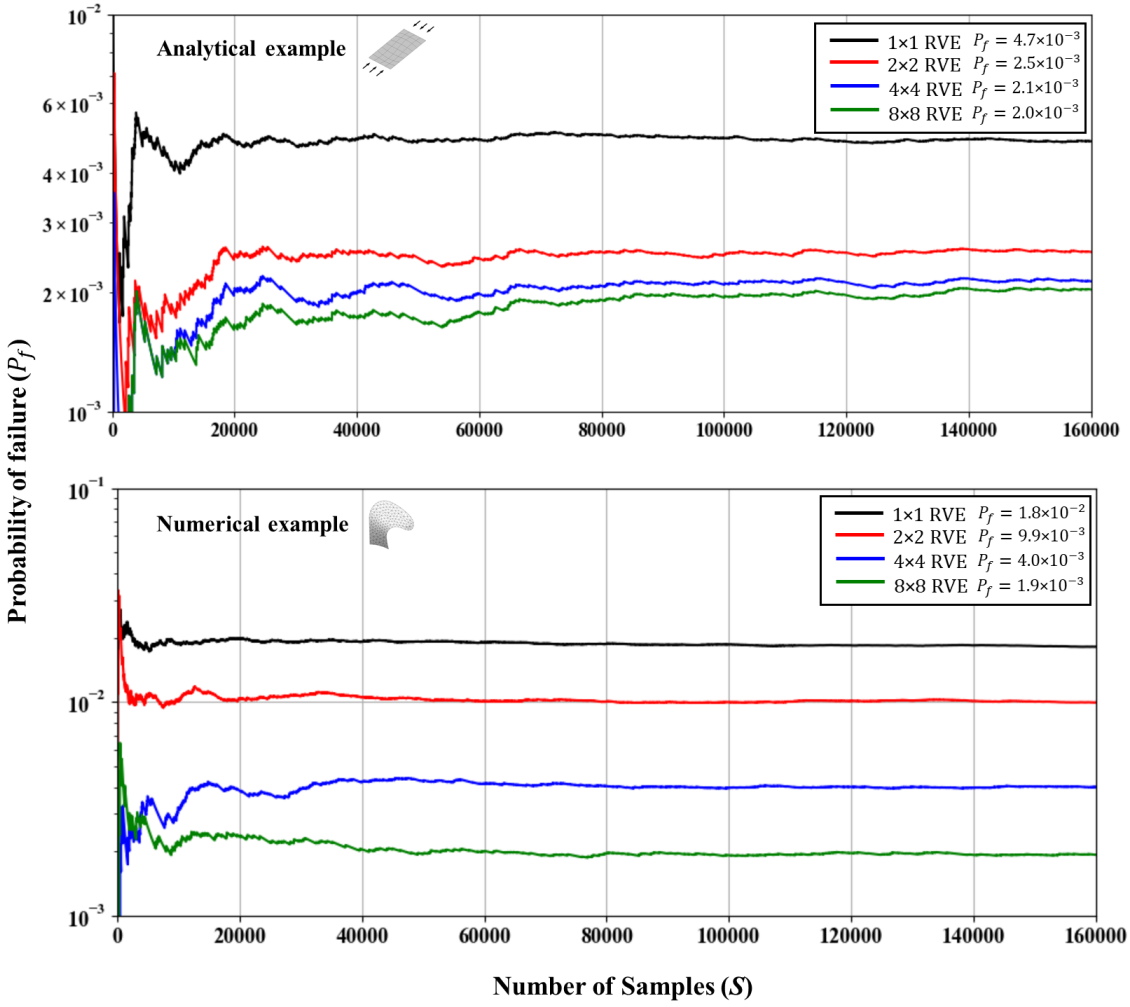

Fig. 15. Probabilities of failure for laminates under micro, meso, and laminate scale uncertainties assessed using various sizes of LRVEs.

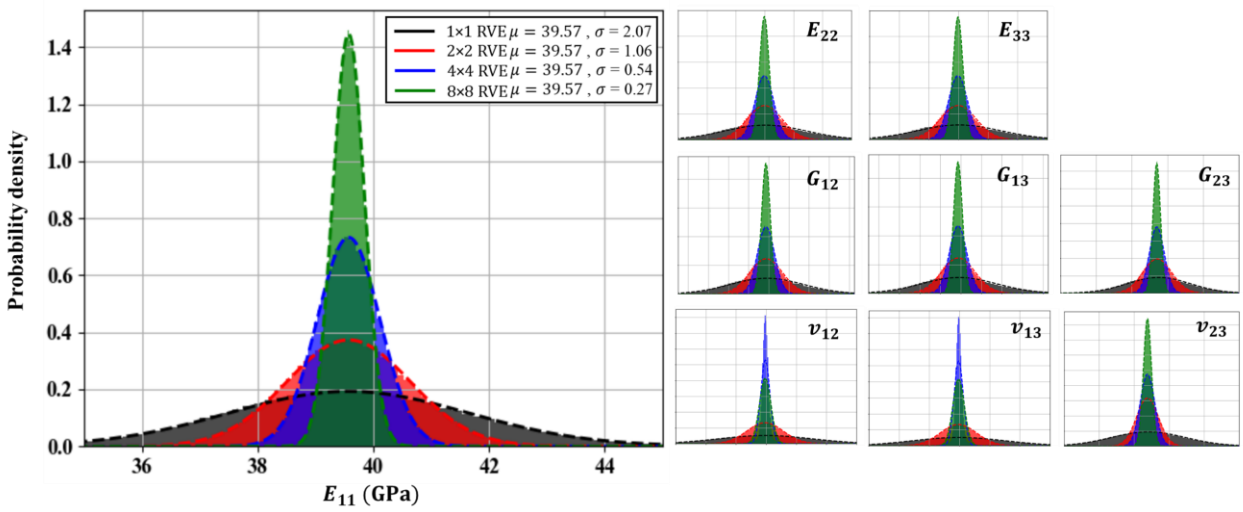

Fig. 16. Distribution of the homogenised LRVEs properties and their fitted normal distribution curve.

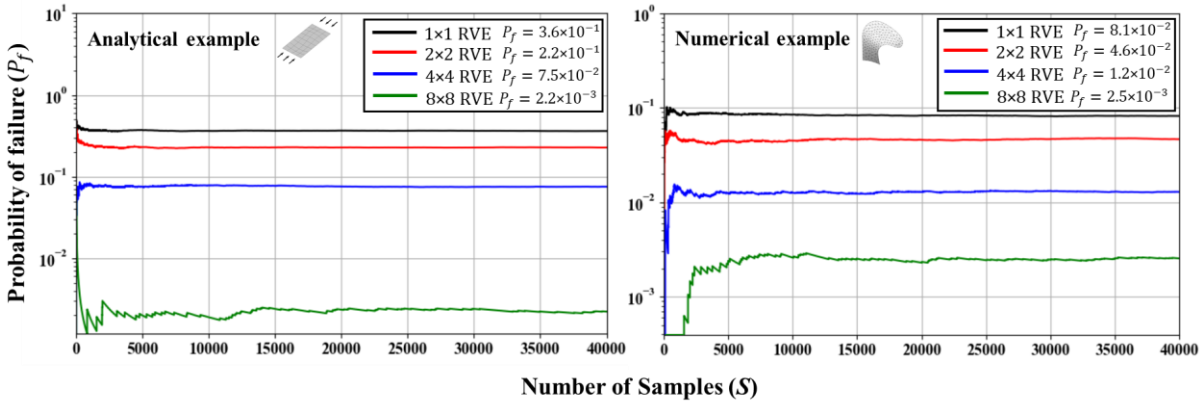

Fig. 17. Probabilities of failure for laminates under micro and meso scale uncertainties assessed using various sizes of LRVEs.

To summarise, as the LRVEs provide a more realistic representation of the material, the computed probability of failure provides a better understanding of the composite components capacity, compared with the use of a more conservative single RVE representation (see Fig. 1).

In terms of computational efficiency, the generation and analysis of the 160,000 MCS samples of the LRVEs, shown in Fig. 15, took less than 10 minutes, while the generation of the FEA homogenisation data points required to interpolate the surrogate models took approximately 20 hours, analysed using a conventional computer with a single core (no parallel computation). It is important to emphasise that the generation of the one-off FEA data points is only required once, for a certain composite material, and they can be used for various applications and reliability analyses (including alterations to the statistical properties of uncertainties). This reduces the reliability analysis time to less than 10 minutes, which is the case for both application examples used in this study. In contrast, the time required to analyse a single deterministic 8×8 high fidelity FEA LRVE using the same machine took approximately 26 hours. Thus, using high-fidelity FEA is not feasible for probabilistic analysis.

5. Conclusions and future work

This study develops a computationally efficient FEA-based surrogate modelling framework capable of capturing various multi-scale uncertainties for continuous fibre reinforced composites. The first step in developing this framework is to use a representative unit that can model spatial variation of uncertainties, compared with a single RVE containing only one or two fibres. This was achieved by constructing an LRVE formed by correlating smaller RVEs in terms of material properties and geometric uncertainties. The second step is to create a series of surrogate models and techniques using a limited number of FEA data points, which propagate between micro and meso-scale, making it feasible to use the LRVE for stiffness reliability calculations using MCS.

The estimated stiffness properties using the developed surrogate modelling technique are validated against FEA samples and the average error is observed to be 0.035% at the micro-scale and 0.22% at the meso-scale. The effect of using LRVEs, compared with the conventional use of a single RVE, in each MCS sample is investigated by computing the reliability of a composite laminate using three different sizes of LRVEs (2×2, 4×4 and 8×8 RVEs) and the established single RVEs (1×1). It is concluded that the use of the LRVE results in a better representation of the uncertainty within the composite and leads to reducing the probability of failure. On the other hand, the proposed framework is efficient for use within a probabilistic method, as an alternative to computationally expensive non-homogenised FEA models and complex analytical methods. Thus, this framework can be used to conduct further probabilistic studies, such as multi-scale reliability-based design optimisation (RBDO) with the possibility of including fibre-matrix interface uncertainty.

Acknowledgements

This work was supported by the University of Aberdeen Elphinstone scholarship scheme.

Appendixes

Appendix A

Displacement relations require linking nodal degrees of freedom (DoF) for periodicity boundary conditions [31]:

For elastic modulus, i.e. E_{11}:

$$U^x_{Front} - U^x_{Back} = U_{Assigned}$$

$$U^x_{Top,\ Left} - U^x_{Bottom,\ Right} = 0$$

$$U^y_{Top,\ Front,\ Left} - U^y_{Bottom,\ Back,\ Right} = 0$$

$$U^z_{Front,\ Top,\ Left} - U^z_{Back,\ Bottom,\ Right} = 0$$

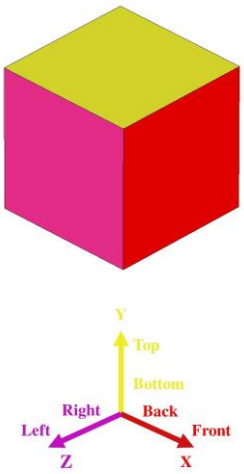

For shear modulus, i.e. G_{12}:

$$U^x_{Front,\ Left} - U^x_{Back,\ Right} = 0$$

$$U^y_{Front} - U^y_{Back} = U_{Assigned}$$

$$U^x_{Top} - U^x_{Bottom} = U_{Assigned}$$

$$U^y_{Top,\ Left} - U^y_{Bottom,\ Right} = 0$$

$$U^z_{Front,\ Top,\ Left} - U^y_{Back,\ Bottom,\ Right} = 0$$

Where U^x, U^y, and U^z are the displacement components along X, Y, and Z direction respectively, $U_{Assigned}$ is the prescribed displacement value for the required modulus.

Appendix B

$$\begin{bmatrix} M_x \\ M_y \\ M_{xy} \end{bmatrix} = \begin{bmatrix} D_{11} & D_{12} & D_{16} \\ D_{12} & D_{22} & D_{26} \\ D_{16} & D_{26} & D_{66} \end{bmatrix} \begin{bmatrix} \mathrm{K}_x \\ \mathrm{K}_y \\ \mathrm{K}_{xy} \end{bmatrix}$$

Where M is the moment per unit width, K is the middle-surface curvature, and D_{ij} are the bending stiffnesses components:

$$D_{\mathrm{ij}} = \frac{1}{3}\sum_{k=1}^{n} \bar{Q}^k_{ij}(t^3_k - t^3_{k-1})$$

Where t_k is the directed distance of the k-th ply, and $\bar{Q}^k_{ij}$ is The k-th layer transformed stiffness coefficients:

$$\bar{Q}^k_{11} = Q_{11}\cos^4\theta^k + 2(Q_{12} + 2Q_{66})\sin^2\theta^k\cos^2\theta^k + Q_{22}\sin^4\theta^k$$

$$\bar{Q}^k_{12} = (Q_{11} + Q_{22} - 4Q_{66})\sin^2\theta^k\cos^2\theta^k + Q_{12}(\sin^4\theta^k + \cos^4\theta^k)$$

$$\bar{Q}^k_{22} = Q_{11}\sin^4\theta^k + 2(Q_{12} + 2Q_{66})\sin^2\theta^k\cos^2\theta^k + Q_{22}\cos^4\theta^k$$

$$\bar{Q}^k_{16} = (Q_{11} - Q_{12} - 2Q_{66})sin\theta^k\cos^3\theta^k + (Q_{12} - Q_{22} + 2Q_{66})sin\theta^k\cos^3\theta^k$$

$$\bar{Q}^k_{26} = (Q_{11} - Q_{12} - 2Q_{66})\sin^3\theta^k cos\theta^k + (Q_{12} - Q_{22} + 2Q_{66})sin\theta^k\cos^3\theta^k$$

$$\bar{Q}^k_{66} = (Q_{11} + Q_{22} - 2Q_{12} - 2Q_{66})\sin^2\theta^k\cos^2\theta^k + Q_{66}(\sin^4\theta^k + \cos^4\theta^k)$$

Where θ^k represents the k-th ply orientation angle, and Q_{ij} are the reduced stiffnesses components:

$$Q_{11} = \frac{E_{11}}{1-\nu_{12}\nu_{21}},\ Q_{12} = \frac{\nu_{12}E_{22}}{1-\nu_{12}\nu_{21}},\ Q_{22} = \frac{E_{22}}{1-\nu_{12}\nu_{21}},\ Q_{66} = G_{12}$$

References

[1] González, C. and LLorca, J., (2007). Mechanical behavior of unidirectional fiber-reinforced polymers under transverse compression: Microscopic mechanisms and modeling, *Composites Science and Technology*, **67** (13), pp.2795-2806.

[2] Sriramula, S. and Chryssanthopoulos, M.K., (2009). *Quantification of uncertainty modelling in stochastic analysis of FRP composites*, *Composites Part A: Applied Science and Manufacturing*, **40**(11), pp.1673-1684. Available at: http://www.sciencedirect.com/science/article/pii/S1359835X09002577

[3] Komeili, M. and Milani, A.S., (2012). The effect of meso-level uncertainties on the mechanical response of woven fabric composites under axial loading, *Computers & Structures*, **90–91** pp.163-171.

[4] Nikopour, H. and Selvadurai, A.P.S., (2014). Concentrated loading of a fibre-reinforced composite plate: Experimental and computational modeling of boundary fixity, *Composites Part B: Engineering*, **60** pp.297-305.

[5] Yancey, R.N., (2016). Challenges, opportunities, and perspectives on lightweight composite structures: Aerospace versus automotive, In Njuguna, J., (Ed.) *Lightweight Composite Structures in Transport*Woodhead Publishing, pp. 35-52.

[6] Qiu, S., Fuentes, C.A., Zhang, D., Van Vuure, A.W. and Seveno, D., (2016). Wettability of a single carbon fiber, *Langmuir*, **32** (38), pp.9697-9705.

[7] Zhang, S., Zhang, L., Wang, Y., Tao, J. and Chen, X., (2016). Effect of ply level thickness uncertainty on reliability of laminated composite panels, *Journal of Reinforced Plastics and Composites*, **35** (19), pp.1387-1400.

[8] Tomar, S.S., Zafar, S., Talha, M., Gao, W. and Hui, D., (2018). *State of the art of composite structures in non-deterministic framework: A review*, *Thin-Walled Structures*, **132**pp.700-716. Available at: http://www.sciencedirect.com/science/article/pii/S0263823117312296

[9] Zhu, T., (1993). A reliability-based safety factor for aircraft composite structures, *Computers & Structures*, **48** (4),

[10] Di Sciuva, M. and Lomario, D., (2003). *A comparison between monte carlo and FORMs in calculating the reliability of a composite structure*, *Composite Structures*, **59**(1), pp.155-162. Available at: http://www.sciencedirect.com/science/article/pii/S0263822302001708

[11] Nicholas, P.E., Padmanaban, K.P. and Sofia, A.S., (2012). *Optimization of dispersed laminated composite plate for maximum safety factor using genetic algorithm and various failure criteria*, *Procedia Engineering*, **38**pp.1209-1217. Available at: http://www.sciencedirect.com/science/article/pii/S1877705812020656

[12] Boyer, C., Béakou, A. and Lemaire, M., (1997). *Design of a composite structure to achieve a specified reliability level*, *Reliability Engineering & System Safety*, **56**(3), pp.273-283. Available at: http://www.sciencedirect.com/science/article/pii/S0951832096000956

[13] Maha, A., Bennett, R.M. and Zureick Abdul-Hamid, (2004). Probabilistic Based Design of Concentrically Loaded Fiber-Reinforced Polymeric Compression Members, *Journal of Structural Engineering*, **130** (12), pp.1914-1920.

[14] Omairey, S.L., Dunning, P.D. and Sriramula, S., (2018). *Influence of micro-scale uncertainties on the reliability of fibre-matrix composites*, *Composite Structures*, **203**pp.204-216. Available at: http://www.sciencedirect.com/science/article/pii/S0263822318313370

[15] Choi, S., Grandhi, R.V. and Canfield, R.A., (2007). *Reliability-based structural design*, Available at:

[16] Chamis, C.,C., (1983). Simplified composite micromechanics equations for hygral, thermal and mechanical properties, *Ann. Conf. of the Society of the Plastics Industry (SPI) Reinforced Plastics/Composites Inst.; 38th; 7-11 Feb. 1983*, Houston, TX; United States,

[17] Mori, T. and Tanaka, K., (1973). *Average stress in matrix and average elastic energy of materials with misfitting inclusions*, *Acta Metallurgica*, **21**(5), pp.571-574. Available at: http://www.sciencedirect.com/science/article/pii/0001616073900643

[18] Cheng, G.-., Cai, Y.-. and Xu, L., (2013). Novel implementation of homogenization method to predict effective properties of periodic materials, *Acta Mechanica Sinica/Lixue Xuebao*, **29** (4), pp.550-556.

[19] El Said, B. and Hallett, S.R., (2018). *Multiscale surrogate modelling of the elastic response of thick composite structures with embedded defects and features*, *Composite Structures*, **200**pp.781-798. Available at: http://www.sciencedirect.com/science/article/pii/S0263822317327587

[20] Hill, R., (1963). *Elastic properties of reinforced solids: Some theoretical principles*, *Journal of the Mechanics and Physics of Solids*, **11**(5), pp.357-372. Available at: http://www.sciencedirect.com/science/article/pii/002250966390036X

[21] Brockenbrough, J.R., Suresh, S. and Wienecke, H.A., (1991). *Deformation of metal-matrix composites with continuous fibers: Geometrical effects of fiber distribution and shape*, *Acta Metallurgica Et Materialia*, **39**(5), pp.735-752. Available at: http://www.sciencedirect.com/science/article/pii/0956715191902745

[22] Babu, K.P., Mohite, P.M. and Upadhyay, C.S., (2018). *Development of an RVE and its stiffness predictions based on mathematical homogenization theory for short fibre composites*, *International Journal of Solids and Structures*, **130-131**pp.80-104. Available at: http://www.sciencedirect.com/science/article/pii/S0020768317304729

[23] Naya, F., Lopes, C.S., González, C. and LLorca, J., (2015). *15 - computational micromechanics strategies for the analysis of failure in unidirectional composites*, pp.411-433. Available at: http://www.sciencedirect.com/science/article/pii/B9780081003329000153

[24] Selvadurai, A.P.S. and Nikopour, H., (2012). Transverse elasticity of a unidirectionally reinforced composite with an irregular fibre arrangement: Experiments, theory and computations, *Composite Structures*, **94** (6), pp.1973-1981.

[25] Yang, L., Wu, Z., Cao, Y. and Yan, Y., (2015). Micromechanical modelling and simulation of unidirectional fibre-reinforced composite under shear loading, *Journal of Reinforced Plastics and Composites*, **34** (1), pp.72-83.

[26] Haeri, A. and Fadaee, M.J., (2016). *Efficient reliability analysis of laminated composites using advanced kriging surrogate model*, *Composite Structures*, **149**pp.26-32. Available at: http://www.sciencedirect.com/science/article/pii/S0263822316302525

[27] Díaz, J., Cid Montoya, M. and Hernández, S., (2016). *Efficient methodologies for reliability-based design optimization of composite panels*, *Advances in Engineering Software*, **93**pp.9-21. Available at: http://www.sciencedirect.com/science/article/pii/S0965997815001738

[28] Sobey, A.J., Blake, J.I.R. and Shenoi, R.A., (2018). Reliability of composite marine structures, In Davies, P. and Rajapakse, Y.D.S., (Eds.) *Durability of Composites in a Marine Environment 2*Cham: Springer International Publishing, pp. 113-134.

[29] Bostanabad, R., Liang, B., Gao, J., Liu, W.K., Cao, J., Zeng, D., Su, X., Xu, H., Li, Y. and Chen, W., (2018). *Uncertainty quantification in multiscale simulation of woven fiber composites*, *Computer Methods in Applied Mechanics and Engineering*, **338**pp.506-532. Available at: http://www.sciencedirect.com/science/article/pii/S0045782518302032

[30] Wu, L., Chung, C.N., Major, Z., Adam, L. and Noels, L., (2018). *From SEM images to elastic responses: A stochastic multiscale analysis of UD fiber reinforced composites, Composite Structures,* **189**pp.206-227. Available at: http://www.sciencedirect.com/science/article/pii/S0263822317327770

[31] Omairey, S.L., Dunning, P.D. and Sriramula, S., (2018). Development of an ABAQUS plugin tool for periodic RVE homogenisation, *Engineering with Computers,* **, 35**(2), pp. 567-577. Available at: https://link.springer.com/article/10.1007/s00366-018-0616-4

[32] Zhang, S., Wang, H., Zhang, L. and Chen, X., (2018). *Statistical correlation between elastic properties of plain-weave composite and its influence on structure reliability, Composite Structures,* **200**pp.939-945. Available at: http://www.sciencedirect.com/science/article/pii/S0263822317342708

[33] Henrik, S.T., Branner, K., Leon Mishnaevsky, J. and John, D.S., (2013). Uncertainty modelling and code calibration for composite materials, *Journal of Composite Materials,* **47** (14), pp.1729-1747.

[34] Sakata, S., Ashida, F. and Enya, K., (2012). *A microscopic failure probability analysis of a unidirectional fiber reinforced composite material via a multiscale stochastic stress analysis for a microscopic random variation of an elastic property, Computational Materials Science,* **62**pp.35-46. Available at: http://www.sciencedirect.com/science/article/pii/S0927025612002789

[35] Xia, Z., Zhang, Y. and Ellyin, F., (2003). *A unified periodical boundary conditions for representative volume elements of composites and applications, International Journal of Solids and Structures,* **40**(8), pp.1907-1921. Available at: http://www.sciencedirect.com/science/article/pii/S0020768303000246

[36] Thode, H.C., (2002). Testing for Normality. Boca Raton: CRC Press.

[37] Kassapoglou, C., (2010). Design and Analysis of Composite Structures : With Applications to Aerospace Structures. Available at: http://ebookcentral.proquest.com/lib/abdn/detail.action?docID=589191.

[38] Reddy, J.,N., (2004). Mechanics of Laminated Composite Plates and Shells: Theory and Analysis. Portland, United States, Portland: Ringgold Inc.

[39] Jones, R.M., (1999). Mechanics of Composite Materials. New York ; London: Brunner-Routledge.

[40] T. E. Oliphant, (2007). Python for Scientific Computing, *Computing in Science & Engineering,* **9** (3), pp.10-20.

[41] Hahn, G.J., (1972). Sample Sizes for Monte Carlo Simulation, *IEEE Transactions on Systems, Man, and Cybernetics,* **SMC-2** (5), pp.678-680.